RSC Advances

PAPER

View Article Online
View Journal | View Issue

Open Access Article. Published on 02 December 2025. Downloaded on 1/15/2026 7:05:29 AM.
This article is licensed under a Creative Commons Attribution-NonCommercial 3.0 Unported Licence.

Check for updates

Cite this: *RSC Adv.*, 2025, **15**, 47452

Polycyclic polyprenylated acylphloroglucinols from the fruit of *Hypericum addingtonii* N. Robson and their α-glucosidase inhibitory activity

Qian Feng,[ab] Rui-Dan Hu,[b] Xian-Feng Xiao,[b] Aijia Ji[b] and Li-Jun Qiao *[a]

Received 21st July 2025
Accepted 4th November 2025

DOI: 10.1039/d5ra05247e

rsc.li/rsc-advances

This paper presents the first chemical investigation of the fruit of *Hypericum addingtonii* N. Robson, leading to the isolation of seven previously undescribed compounds and 14 known polycyclic polyprenylated acylphloroglucinols. The seven unreported compounds included four terpenoidal polycyclic polyprenylated acylphloroglucinols, hypertonii A–D (**1–4**), and three anthrone derivatives, hyperxanthone G–H (**19–21**). The structures of the undescribed compounds were confirmed using spectroscopic analyses, electronic circular dichroism, and nuclear magnetic resonance calculations. The α-glucosidase inhibitory activities of all the isolated compounds were evaluated. Fifteen compounds showed remarkable activity with half maximal inhibitory concentrations (IC_{50}) ranging from 1.13 ± 0.26 to 42.7 ± 9.00 μM. The most active compound (**7**) showed strong activity (IC_{50} = 1.13 ± 0.26 μM), and compounds **11**, **1**, **12**, and **18** displayed considerable activity (IC_{50} = 2.85 ± 0.15, 3.03 ± 0.15, 3.16 ± 0.21, and 3.55 ± 0.45 μM, respectively). Kinetic studies showed that the five most active compounds were mixed-type α-glucosidase inhibitors. Molecular docking analysis revealed that these active compounds had good binding affinity to α-glucosidase.

1. Introduction

Hypericum addingtonii N. Robson is a shrub that belongs to the Hypericaceae family, which is widely distributed over Southwest and South China.[1] Previous studies have demonstrated that natural products,[2,3] such as terpenoidal phloroglucinol derivatives from the Hypericaceae family, are important in finding new α-glucosidase inhibitors.[4–7] Diabetes mellitus is a chronic health condition characterized by high blood glucose levels, which lead to major complications such as cardiovascular disease, retinopathy, and kidney disease. Diabetes mellitus is classified into type 1 and type 2 based on its etiology. About 90–95% of patients with diabetes have type 2 diabetes mellitus (T2DM),[8,9] which develops when the body becomes resistant to insulin. Glycemic control is effective for preventing complications associated with diabetes.[10] α-Glucosidase, an enzyme that breaks down carbohydrates into glucose, plays an important role in glycemic regulation. α-Glucosidase inhibitors can reduce intestinal glucose production and absorption, making them a promising treatment for T2DM.[11] There has been growing interest in plant-derived α-GC inhibitors, with numerous recent studies focusing on polycyclic polyprenylated acylphloroglucinols (PPAPs) isolated from the *Hypericum* and *Garcinia* genera.[11]

To identify new α-glucosidase inhibitors from the Clusiaceae family, a chemical analysis of the fruit of *Hypericum addingtonii* N. Robson was conducted. Seven new compounds, including four terpenoidal phloroglucinol derivatives (**1–4**), and three anthrone derivatives (**19–21**), were isolated along with 14 known terpenoidal phloroglucinol derivatives (uralione B (**5**),[12] uralodin B (**6**),[13] uralodin C (**7**),[14] hyperibone A (**8**),[15] hyperattenins A (**9**),[14] sampsoniones M (**10**),[16] hyperisampsins (**11**),[17] hyperisampsins H (**12**),[17] otogirinin B (**13**),[18] hyperisampsin N (**14**),[17] attenuatumione D (**15**),[19] sampsonione C (**16**),[16] sampsonione L (**17**)[16] and iotogirinin D (**18**)[18]). Their structural elucidations are described herein. Moreover, the α-glucosidase inhibitory activity of all isolated compounds, along with their inhibitory kinetic analysis and interactions with α-glucosidase, are reported.

2. Results and discussion

2.1 Structural elucidation of the new compounds

Hypertonii A (**1**) was a yellowish oil. Its formula ($C_{35}H_{44}O_6$) was deduced from the $[M + H]^+$ ion peak at *m/z* 561.3210 and the ^{13}C-NMR data. The ^{1}H-NMR data of compound **1** (Table 1) showed five benzene ring protons [δ_H 7.12–7.42 (5H, m)], two double bond protons [δ_H 5.05 (1H, t, *J* 5.8), 5.24 (1H, t, *J* 7.4)], and seven methyl protons [δ_H 1.42, 1.40, 1.24, 1.17, 1.58 (each 3H, s), and 1.66 (6H, s)]. The ^{13}C-NMR, distortionless enhancement by

[a]*State Key Laboratory of Traditional Chinese Medicine Syndrome, The Second Affiliated Hospital of Guangzhou University of Chinese Medicine, Guangzhou 510405, China. E-mail: qiaolijunwork@163.com*

[b]*International Institute for Translational Chinese Medicine, School of Pharmaceutical Sciences, Guangzhou University of Chinese Medicine, Guangzhou, China*

© 2025 The Author(s). Published by the Royal Society of Chemistry

Open Access Article. Published on 02 December 2025. Downloaded on 1/15/2026 7:05:29 AM.
This article is licensed under a Creative Commons Attribution-NonCommercial 3.0 Unported Licence.

Table 1 ^{1}H NMR data of **1–4** in $CDCl_3$ (400 MHz)

No.	**1** (*J* Hz)	**2** (*J* Hz)	**3** (*J* Hz)	**4** (*J* Hz)
5	—	1.50, m	—	—
6	—	1.63, m; 1.50, m	—	—
7	2.00, m; 3.05, dd (13.1, 8.7)	1.62, m; 2.25, m	1.46, m; 1.99, m	2.01, m
8	4.31, dd (8.7, 7.4)	1.14, m	1.90, m	1.86, m
9	—	—	—	—
10	4.22, t (8.4)	3.19, m	2.18, m	2.12, m
11	2.13, m; 2.37, m	1.36, m; 1.63, m	4.97, m	4.95, m
12	2.04, m	1.30, m; 1.44, m	—	—
13	—	—	1.67, s	1.68, s
14	2.00, m; 2.56, m	1.18, s	1.56, s	1.57, s
15	1.41, s	0.73, s	1.90, m; 2.05, m	1.50, m; 2.39, m
16	1.24, s	1.00, s	1.32, m; 1.48, m	1.72, m
17	1.40, s	—	3.27, dd (10.1, 1.9)	3.26, dd (9.8, 1.9)
18	1.17, s	1.10, s	—	—
19	2.60, d (7.4)	1.25, s	1.26, s	1.24, s
20	5.24, t (7.4)	5.09, m	1.20, s	1.24, s
21	—	—	2.08, m	2.07, m
22	2.03, m	1.60, s	3.55, m	3.55, m
23	2.03, m; 2.11, m	1.74, s	—	—
24	5.05, t (5.8)	0.97, s	1.26, s	1.21, s
25	—	2.33, m	1.24, s	1.21, s
26	1.58, s	2.77, m	2.61, qd (17.3, 4.3)	2.61, qd (17.3, 4.3)
27	1.66, s	5.14, m	3.63, t (4.3)	3.63, t (4.3)
28	1.65, s	—	—	—
29	—	1.72, s	1.23 s	1.21 s
30	—	1.64, s	0.53, s	0.54, s
31	7.31, m	—	—	—
32	7.12, m	—	—	—
33	7.42, m	8.00, m	7.67, m	7.68, m
34	7.12, m	7.44, m	7.33, m	7.31, m
35	7.31, m	7.53, m	7.43, m	7.43, m
36		7.44, m	7.33, m	7,31, m
37		8.00, m	7.67, m	7.68, m
38			1.26, s	1.21, s

polarization transfer (DEPT-135), and heteronuclear single quantum coherence spectroscopy (HSQC) spectra revealed 35 carbon signals, including 7 methyl, 6 methylene, and 10 methine groups, as well as 12 quaternary carbons. The NMR data (Tables 1 and 2) of **1** were compared with those of the known compound hyperattenin H.[17] The major differences between compound **1** and hyperattenin H were the chemical shifts of C-9 (δ_C 72.6 for **1** *vs.* δ_C 48.8 for hyperattenin H), C-10 (δ_C 81.7 for **1** but δ_C 51.9 for hyperattenin H), and C-11 (δ_C 31.4 for **1** *vs.* δ_C 22.8 for hyperattenin H). This suggested that C-9 and C-10 may be connected *via* an oxygen atom (Fig. 1). The correlated spectroscopy (^{1}H–^{1}H COSY, Fig. 2) cross-peak of H-8 (δ_H 4.31, 1H, dd, *J* 8.6, 7.4)/H_2-7 (δ_H 2.02, 1H, m and 3.05, 1H, dd, *J* 13.1, 8.6), along with the heteronuclear multiple bond correlation (HMBC, Fig. 2) cross-peaks from Me-15 (δ_H 1.17, 3H, s)/Me-16 (δ_H 1.24, 3H, s) to C-8, C-9, and C-10, from H-10 (δ_H 4.22, 1H, t, $J = 8.4$) to C-14 and C-13, indicated a pyrane ring unit.

The rotating-frame Overhauser effect spectroscopy (ROESY) cross-peaks of H-7 (δ_H 2.02)/H-32 (δ_H 7.12) indicated that H-7 and H-32 had the same face orientation, which was identified as β-oriented. This suggested that the benzoyl group attached at C-3 was β-oriented. Furthermore, the H-7β/H-10/H-14 correlations indicated that H-14 and H-10 had different orientations. The correlations between H-7 and H-5 indicated that the C-8 hydroxyl was α-oriented. Thus, the relative configuration of **1** (1*R**, 3*R**, 8*R**, 10*S**, 12*S**, 13*R**) was assigned.

ECD calculations were used to verify the configuration of compound **1**. As shown in Fig. 3, the calculated ECD curve of (1*R*, 3*R*, 8*R*, 10*S*, 12*S*, 13*R*)-**1** was in good agreement with the experimental curve. Finally, the complete structure of **1** was elucidated.

Hypertonii B (**2**) was obtained as a colorless oil. Its molecular formula ($C_{37}H_{52}O_4$) was determined from the $[M + H]^+$ ion peak at *m*/*z* 561.3938 and the ^{13}C-NMR spectrum. The ^{1}H NMR data of **2** (Table 1) showed five benzene ring protons [δ_H 7.44–8.00 (5H, m)], two double bond protons [δ_H 5.10 (1H, m), 5.14 (1H, m)], and nine methyl protons [δ_H 1.74, 1.71, 1.64, 1.60, 1.18, 1.10, 1.00, 0.97 and 0.72 (each 3H, s)]. The ^{13}C NMR, DEPT-135, HSQC, and HMBC spectra showed 37 carbons attributed to an isopentene group [δ_C 18.0 (C-22); 25.9 (C-23); 29.7 (C-19); 123.0 (C-20); 133.1 (C-21)], a benzoyl group, an acetyl group [δ_C 211.9 (C-17); 27.1 (C-18)], a 4-methylpen-3-en-1-yl moiety [δ_C 22.4 (C-25); 38.7 (C-26); 123.0 (C-27); 133.0 (C-28); 25.8 (C-29); 17.7 (C-30)], and four methyl groups [δ_C 19.1 (C-14); 15.0 (C-15); 27.2 (C-16); 21.9 (C-24)]. These data were similar to the spectral data

Open Access Article. Published on 02 December 2025. Downloaded on 1/15/2026 7:05:29 AM.
This article is licensed under a Creative Commons Attribution-NonCommercial 3.0 Unported Licence.

Table 2 ^{13}C NMR data of **1–4** in $CDCl_3$ (100 MHz)

No.	1	2	3	4
1	76.6, C	53.0, C	63.6, C	63.5, C
2	200.8, C	148.1, C	210, C	210, C
3	81.2, C	133.0, C	73.0, C	73.0, C
4	204.2, C	38.4, C	165.9, C	165.9, C
5	47.8, C	43.4, CH	111.7, C	111.8, C
6	201.3, C	34.8, CH_2	194.8, C	194.8, C
7	32.7, CH_2	28.1, CH_2	42.4, CH_2	42.5, CH
8	87.6, CH	49.7, CH	43.7, CH	44.0, CH
9	72.6, C	37.4, C	50.2, C	50.3, C
10	81.7, CH	77.9, CH	28.0, CH_2	28.1, CH_2
11	31.4, CH_2	28.7, CH_2	122.3, CH	122.2, CH
12	41.5, CH	37.6, CH_2	133.7, C	133.8, C
13	67.8, C	81.1, C	25.8, CH_3	25.9, CH_3
14	35.5, CH_2	19.1, CH_3	18.0, CH_3	18.0, CH_3
15	24.7, CH_3	15.0, CH_3	35.0, CH_2	35.7, CH_2
16	26.8, CH_3	27.2, CH_3	28.8, CH_2	28.6, CH_2
17	22.8, CH_3	211.9, C	79.2, CH	79.8, CH
18	24.5, CH_3	27.1, CH_3	73.3, C	73.2, C
19	28.9, CH_2	29.7, CH_2	26.8, CH_3	26.3, CH_3
20	118.5, CH	123.0, CH	23.6, CH_3	23.7, CH_3
21	139.3, C	133.1, C	32.5, CH_2	32.5, CH_2
22	40.0, CH_2	18.0, CH_3	74.8, CH	74.8, CH
23	26.6, CH_2	25.9, CH_3	73.3, C	73.3, C
24	124.1, CH	21.9, CH_3	24.1, CH_3	24.1, CH_3
25	131.5, C	22.4, CH_2	25.9, CH_3	25.8, CH_3
26	17.7, CH_3	38.7, CH	25.2, CH_2	25.3, CH_2
27	25.8, CH_3	123.0, CH	67.7, CH	67.8, CH
28	16.4, CH_3	133.0, C	82.3, C	82.4, C
29	192.4, C	25.8, CH_3	22.8, CH_3	22.4, CH_3
30	134.9, C	17.7, CH_3	23.5, CH_3	23.5, CH_3
31	128.4, CH	199.2, C	194.2, C	194.5, C
32	128.6, CH	139.2, C	137.5, C	137.6, C
33	132.4, CH	129.4, CH	128.3, CH	128.3, CH
34	128.6, CH	128.3, CH	128.1, CH	128.1, CH
35	128.4, CH	132.7, CH	132.2, CH	132.2, CH
36	—	128.3, CH	128.1, CH	128.1, CH
37	—	129.4, CH	128.3, CH	128.3, CH
38	—	—	13.3, CH_3	13.3, CH_3

of garciniacowone K,[20] except for the resonance of C-10 (δ_C 41.2 for garciniacowone K *vs.* δ_C 77.9 for compound **2**). Based on the above results, a hydroxyl group was deduced to be attached at C-10.

The relative stereochemistry of **2** was deduced using the ROESY spectrum. The correlation between H-10 (δ_H 3.19) and H-8 (δ_H 1.13) suggested the same orientation of H-10 and H-8, which was assigned as α-orientation. The methyl attached at C-4 and the acetyl located at C-1 were both β-oriented based on the correlations between H_2-19 (δ_H 2.26), Me-24 (δ_H 0.97), and Me-18 (δ_H 1.10). The methyl of C-13 was β-oriented based on the correlations of Me-14 (δ_H 1.18), and Me-18 (δ_H 1.10). Therefore, the relative configuration of **2** was deduced as 1*S**, 4*S**, 5*R**, 8*R**, 10*R**, 13*R**. ECD calculations were used to confirm the absolute configuration of **2**. From the results shown in Fig. 3, the calculated ECD curve of (1*S*, 4*S*, 5*R*, 8*R*, 10*R*, 13*R*)-**2** was in good agreement with the experimental ECD curve. Thus, the structure of **2** was confirmed.

Hypertonii C (**3**) and hypertonii D (**4**) were both yellowish oils. High-resolution electrospray ionization mass spectrometry (HR-ESI-MS) showed the same $[M + H]^+$ ion peaks at *m/z* 655.3857, giving the same formula of $C_{38}H_{54}O_9$. The ^{1}H NMR data revealed five benzene ring protons [δ_H 7.33–7.67 (5H, m)], one double bond proton [δ_H 4.97 (1H, m)], and nine methyl protons [δ_H 1.67, 1.56, 1.26, 1.24, 1.23, 1.21, 0.53 (each 3H, s), and 1.20 (6H, s)]. Based on the analyses of the ^{13}C NMR and HSQC spectra, **3** was concluded to have one benzene ring, three keto – carbonyl groups (δ_C 210.0, 194.8, and 194.2), and two double bonds, including one tetrasubstituted (δ_C 111.7 and 165.9) and one trisubstituted [δ_H 4.97 (1H, m), δ_C 122.3 and 133.7]. The NMR data were similar to the known compound uralione B (compound **5**).[5] The major differences between compounds **3** and **5** were the chemical shifts, which were attributed to C-17 and C-18 based on the HMBC spectrum. Compared with **5**, **3** shifted to the lower field (from δ_C 124.7 to δ_C 79.2 of C-17 and from δ_C 131.4 to δ_C 73.3 of C-18), suggesting a missing double bond in **3**. Moreover, C-17 and C-18 were considered to be attached to a hydroxyl group based on their chemical shift and the molecular formula. The above supposition was verified using the ^{1}H–^{1}H COSY correlations of H-15/H-16/H-17 and the HMBC correlation from Me-19/Me-20 to C-17 and C-18 (Fig. 2). By comparing the spectral data of **3** and **4**, the differences were around C-15 (δ_C 35.0 for **3** *vs.* δ_C 35.7 for **4**), C-16 (δ_C 28.8 for **3** *vs.* δ_C 28.6 for **4**), and C-17 (δ_C 79.2 for **3** *vs.* δ_C 79.8 for **4**), indicating that compounds **3**, and **4** were a pair of epimers of C-17.

ROESY experiments were used to determine the relative configurations of **3** and **4**. ROESY correlations (Fig. 3) of Me-30/H-27/H-37/H-33 indicated that these protons were β-oriented. According to the literature,[5] when H-8 is α-oriented, the chemical shift of C-7 ranges from 41 to 44 ppm, and the chemical shift difference between H-7β and H-7α is always from 0.3 to 1.2 ppm. In contrast, when H-8 is β-oriented, the chemical shift of C-4 is from 45 to 49 ppm, and the chemical shift difference between H-7β and H-7α is always from 0.0 to 0.2 ppm. Based on the chemical shift of C-7 (δ_C 43.7) and the chemical shift difference between H-7β and H-7α ($\Delta\delta = \sim 0.56$), H-8 was assigned to the α-orientation. Furthermore, the correlations between H_2-21 and H-11 indicated that H_2-21 was β-oriented. The correlation between H-15/H-8 indicated that H-15 was α-oriented. Finally, based on ROESY cross-peaks of H-7α/H-8 and H-22/H-7α, H-22 was assigned as α-oriented. Based on the above evidence, the relative configuration of **3** was assigned as 1*S**, 3*S**, 8*S**, 9*R**, 22*S**, 27*S**. The absolute configuration of the 17,18-diol motif in **3** and **4** were assigned using the *in situ* dimolybdenum induced CD method. Upon addition of dimolybdenum tetraacteate $[Mo_2(OAc)_4]$ to **3** and **4** in DMSO solution, respectively. The negative Cotton effect observed at around 300 nm in induced CD of **3**, and positive Cotton effect observed at around 330 nm of **4**, consistent with a 17*R*-configuration of **3** and 17*S* of **4** according to the empirical helicity rule.[21,22] (Fig. 3e and f). This deduction was subsequently confirmed by comparing the experimented and calculated ECD curves. The calculated curves of **3** and **4** were both in good agreement with the experimental curves (Fig. 3), thus the absolute configurations of **3** and **4** were determined as 1*S*, 3*S*, 8*S*, 9*R*, 17*R*, 22*S*, 27*S* and 1*S*, 3*S*, 8*S*, 9*R*, 17*S*, 22*S*, 27*S*.

 © 2025 The Author(s). Published by the Royal Society of Chemistry

Open Access Article. Published on 02 December 2025. Downloaded on 1/15/2026 7:05:29 AM.
This article is licensed under a Creative Commons Attribution-NonCommercial 3.0 Unported Licence.

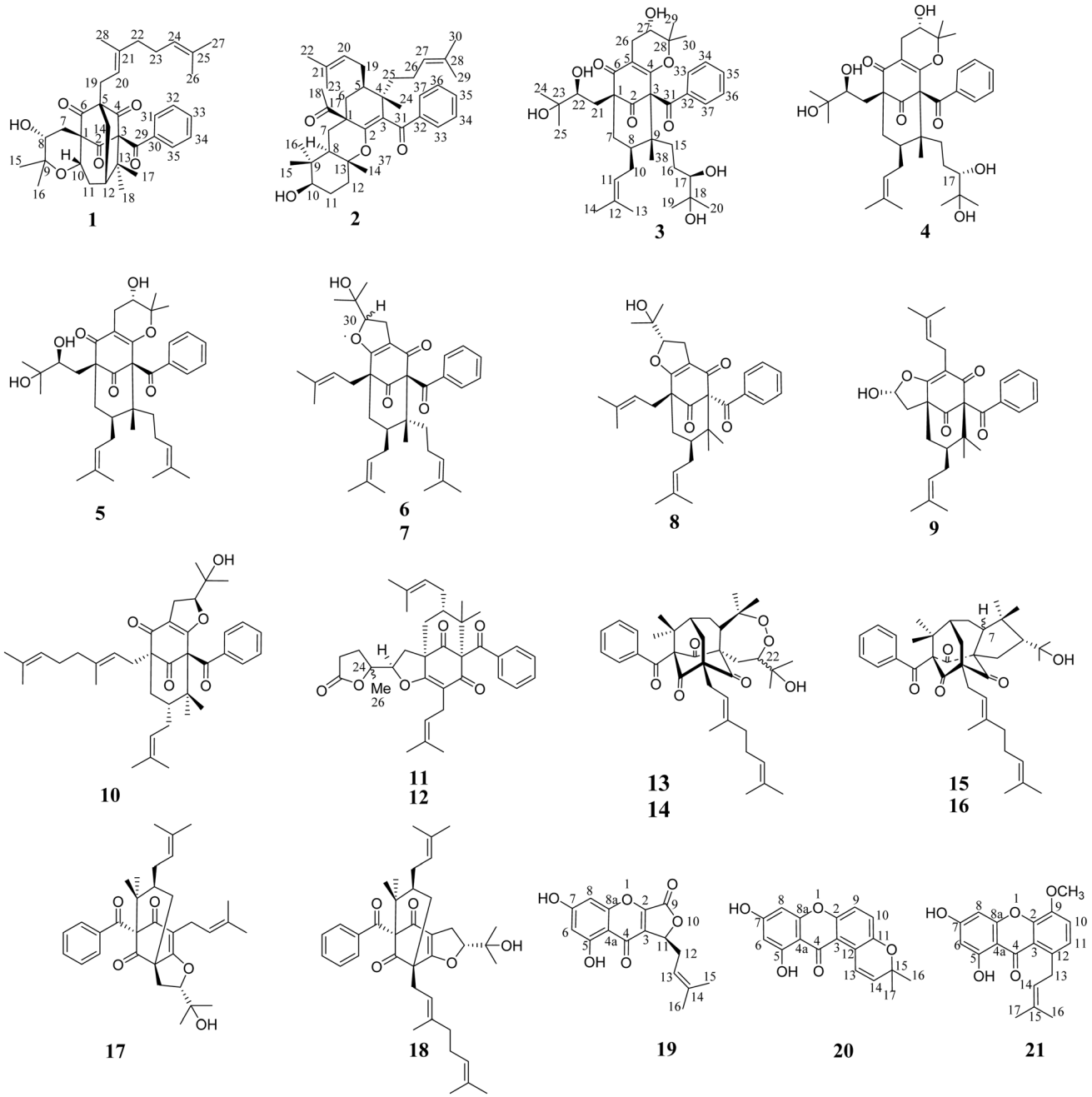

Fig. 1 Chemical structures of **1**–**21**.

Hyperxanthone G (**19**) was obtained as a yellowish powder. Its formula ($C_{16}H_{14}O_6$) was determined from the $[M - H]^-$ peak at *m*/*z* 301.0716 and the ^{13}C NMR data, with an index of hydrogen deficiency (IHD) of 10. The ^1H and ^{13}C NMR spectra showed a 1,2,3,5-tetrasubstituted aromatic ring [δ_H 6.59 (1H, d, *J* 2.2 Hz), 6.39 (1H, d, *J* 2.2 Hz), δ_C 165.5, 162.9, 158.9, 106.0, 100.2, 95.2], a chelated hydroxyl signal at δ_H 12.19, a typical carbonyl signal at δ_C 178.3, and a tetrasubstituted double bond [δ_C 131.5 and 149.9]. The above data of **19** were similar to those of solieritide A,[23] without the obvious signals of an isoprenyl group [δ_H 1.64 (3H, s), 1.67 (3H, s), and 5.15 (1H, dd *J* 7.3, 1.4 Hz); δ_C 30.2, 116.5, and 136.5] observed in **19**. The ^1H–^1H COSY correlations between H-11/H-12/H-13 indicated that the isopentene group was attached at C-11. Thus, the planar structure of **19** was confirmed. ECD calculations were used to determine the configuration of **19**. As shown in Fig. S2, the configuration of **19** was confirmed to be 11*S*.

Hyperxanthone H (**20**) was a yellowish powder. Its formula ($C_{18}H_{16}O_5$) was deduced using (+)-HRESIMS (IHDs = 12). After a comprehensive analysis of the NMR spectrum, compound **20** was considered an anthrone derivative. The ^1H and ^{13}C NMR showed 12 substantial benzene rings [δ_C 103.5–164.4], including a 1, 2, 3, 5-tetrasubstituted aromatic ring, a carbonyl group (δ_C 183.1), and a double bond [δ_H 8.04 (1H, d, *J* 10.2 Hz),

Open Access Article. Published on 02 December 2025. Downloaded on 1/15/2026 7:05:29 AM.
This article is licensed under a Creative Commons Attribution-NonCommercial 3.0 Unported Licence.

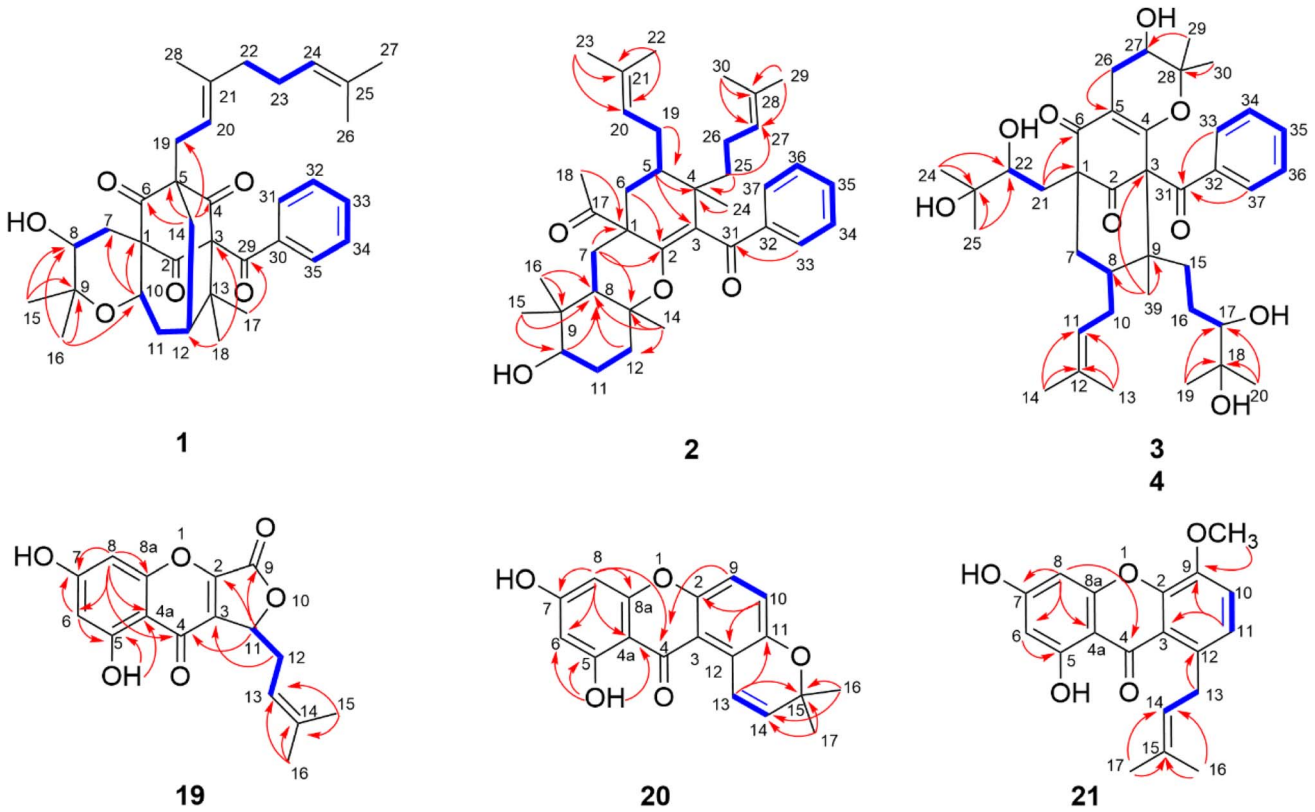

Fig. 2 Key $^{1}H-^{1}H$ COSY and HMBC correlations of **1–4** and **19–21**.

5.94 (1H, d, J 10.2 Hz), δ_C 120.4, 132.9]. The above data were similar to that of toxyloxanthone B,[24] in addition to the different chemical shifts of C-9 (δ_C 124.4 for **20** *vs.* δ_C 153.7 for toxyloxanthone B), C-10 (δ_C 117.9 for **20** *vs.* δ_C 103.1 for toxyloxanthone B), and C-2 (δ_C 151.6 for **20** *vs.* δ_C 138.4 for toxyloxanthone B). This suggested that the hydroxy group of C-9

Table 3 NMR data of **19–21** in $(CD_3)_2CO$ (400 MHz for ^{1}H; 100 MHz for ^{13}C)

	19 (J Hz)		**20** (J Hz)		**21** (J Hz)	
Position	δ_H	δ_C	δ_H	δ_C	δ_H	δ_C
1	—	—	—	—	—	—
2	—	149.9, C	—	151.6, C	—	153.7, C
3	—	131.5, C	—	119.7, C	—	128.7, C
4	—	178.3, C	—	183.1, C	—	183.2, C
4a	—	106.0, C	—	103.5, C	—	103.3, C
5	—	163.0, C	—	164.0, C	—	164.1, C
6	6.39, d (2.2)	100.2, CH	6.23, d (2.2)	98.0, CH	6.22, d (2.1)	97.8, CH
7	—	165.5, C	—	165.4, C	—	165.2, C
8	6.59, d (2.2)	95.2, CH	6.36, d (2.2)	93.2, CH	6.34, d (2.1)	93.0, CH
8a	—	158.9, C	—	157.5, C	—	157.4, C
9	—	162.9, C	7.24, d (9.0)	124.4, CH	—	151.5, C
10	—	—	7.33, d (9.0)	117.9, CH	7.52, d (9.2)	119.1, CH
11	5.61, dd (6.7, 3.7)	78.2, CH	—	149.7, C	7.37, d (9.2)	116.0, CH
12	2.99, m; 2.66, m	30.2, CH_2	—	114.7, C	—	118.4, C
13	5.15, dd (7.3, 1.4)	116.5, CH	8.04, d (10.2)	120.4, CH	4.16, d (6.9)	25.1, CH_2
14	—	136.5, C	5.94, d (10.2)	132.9, CH	5.24, t (6.9)	123.2, CH
15	1.64, s	17.1, CH_3	—	75.3, C	—	130.7, C
16	1.67, s	25.0, CH_3	1.45, s	26.6, CH_3	1.64, s	25.1, CH_3
17	—	—	1.45, s	26.6, CH_3	1.82, s	17.3, CH_3
5-OH	12.19, s	—	13.17, s	—	13.32, s	—
–OMe	—	—	—	—	3.92, s	56.1, CH_3

 © 2025 The Author(s). Published by the Royal Society of Chemistry

Open Access Article. Published on 02 December 2025. Downloaded on 1/15/2026 7:05:29 AM.
This article is licensed under a Creative Commons Attribution-NonCommercial 3.0 Unported Licence.

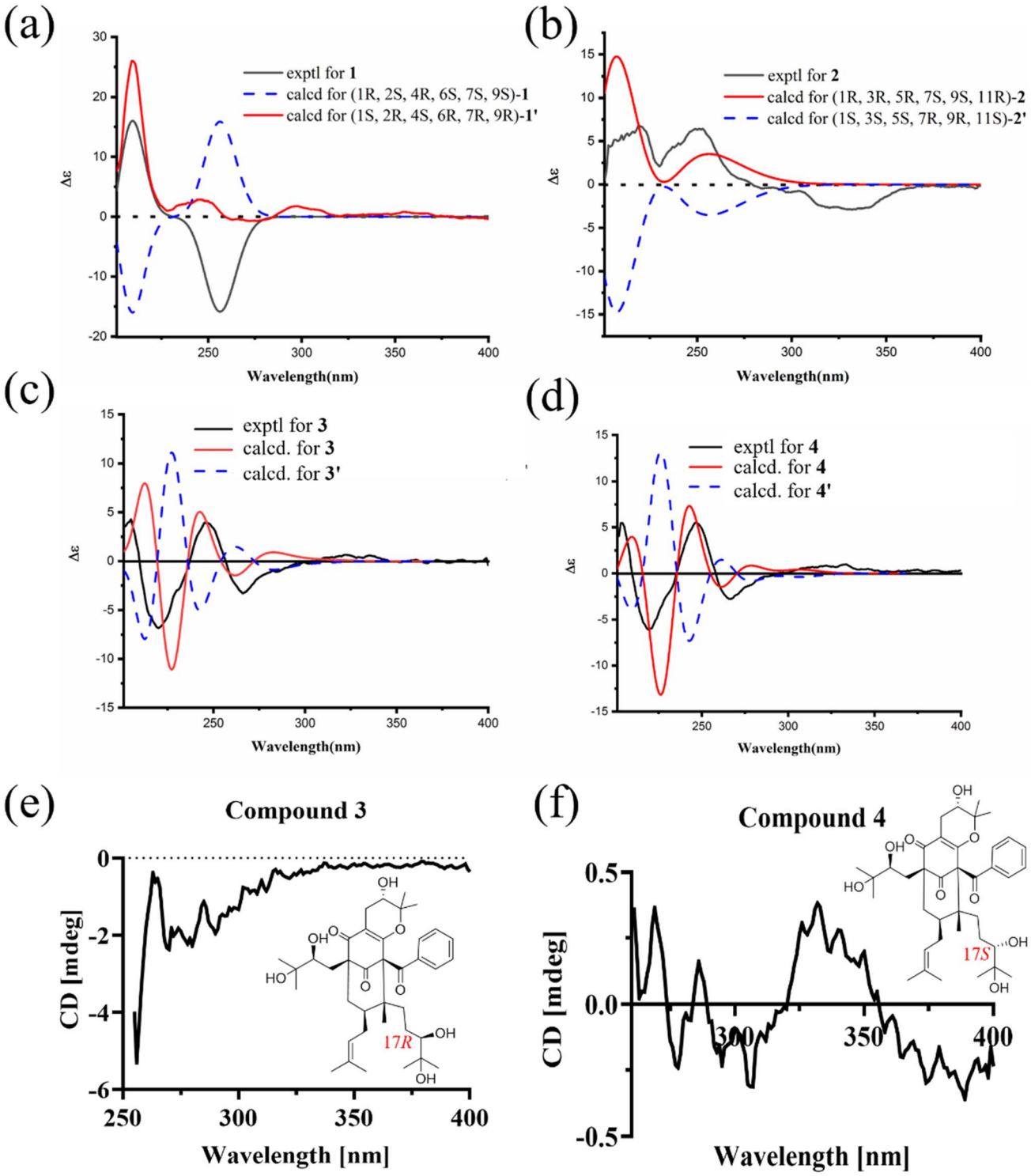

Fig. 3 Experimental and calculated ECD spectra of **1**–**4** (a–d), CD spectra of the $[Mo_2(OAc)_4]$ complexes of compounds **3** (e) and **4** (f).

in toxyloxanthone B was lost in compound **20**. Thus, the structure of **20** was characterized.

Hyperxanthone I (**21**) was a yellowish powder. The formula of **21** ($C_{19}H_{18}O_5$) was deduced from the $[M + H]^+$ ion peak at *m*/*z* 327.1225 (IHD = 11). The ^1H and ^{13}C NMR data of **21** were similar to those of **20**. The NMR data of **21** also showed a typical keto – carbonyl group (δ_C 183.2), 12 aromatic hydrocarbon signals, and a substantial chelated hydroxyl group proton [δ_H 13.32 (s, 1H)], indicating that compound **21** was an anthrone derivative similar to **20**. In addition to an anthrone skeleton, the ^1H–^1H COSY correlation of H-13 and H-14 and the HMBC cross-peaks from Me-17 and Me-16 to C-14, from H-13 to C-12 indicated that an isopentene group was attached at C-12. Furthermore, the HMBC cross-peaks from 18-OMe to C-9 indicated that

Open Access Article. Published on 02 December 2025. Downloaded on 1/15/2026 7:05:29 AM.
This article is licensed under a Creative Commons Attribution-NonCommercial 3.0 Unported Licence.

C-9 was substituted by a methoxy group, which differed from the known compound 1,3,5-trihydroxy-8-isoprenylxanthone.[24] Thus, the structure of **21** was characterized.

2.2 Bioactivity evaluation

2.2.1 α-Glucosidase inhibitory activity. The α-glucosidase inhibitory activities of all isolated compounds were evaluated, as shown in Fig. 4 and Table 4. Fifteen compounds showed considerable α-glucosidase inhibitory activities, five of which were better than acarbose (half maximal inhibitory concentration (IC_{50}) = 3.70 ± 0.20 μM). The most active compound (**7**) showed remarkable activity (IC_{50} = 1.13 ± 0.26 μM). Compounds **11**, **1**, **12**, and **18** displayed strong inhibitory activities (IC_{50} values of 2.85 ± 0.15, 3.03 ± 0.15, 3.16 ± 0.21, and 3.55 ± 0.45 μM, respectively), which were stronger than that of acarbose. Moreover, compounds **6**, **9**, **10**, **14**, **15**, and **16** showed excellent α-glucosidase inhibitory activities with IC_{50} values <10 μM.

2.2.1.1 Kinetic analysis. The α-glucosidase inhibition type of compounds **1**, **7**, **11**, **12**, and **18** and their inhibition constants (K_i values) were studied (Fig. 5). The kinetic results demonstrated that all compounds showed mixed-type inhibition (when the inhibitor concentration increased, V_{max} decreased and K_m increased),[25] indicating that these compounds could bind to α-glucosidase and the α-glucosidase–*p*-NPG complex as well. The K_i value of the most active compound (**7**) was 4.265 μM, whereas those of compounds **1**, **11**, **12**, and **18** were 21.41, 9.208, 6.548, and 8.415 μM, respectively (Fig. 6).

2.2.2 Molecular docking analysis. The structure–activity relationships were further analyzed using molecular docking analysis. As shown in Fig. 7, compound **7**, with the best activity, not only formed hydrogen bonds with residues Asn277 and Lys242, but also interacted with Trp6, Thr253, Ala247, Phe246, Lys4, Ile251, and Glu71. Compound **1** mainly interacted with Trp6, Asn277, Lys4, Ala2447, and Lys242, which were the same residues interacting with compound **7**. Compound **11** mainly interacted with Met184, Asp70, Pro109, His108, and Tyr68, whereas compound **12** mainly interacted with Tyr552, Arg550, Leu533, Val526, Thr538, *etc.* Compound **18** formed a hydrogen bond with Ile143, and mainly interacted with Leu19, Glu141,

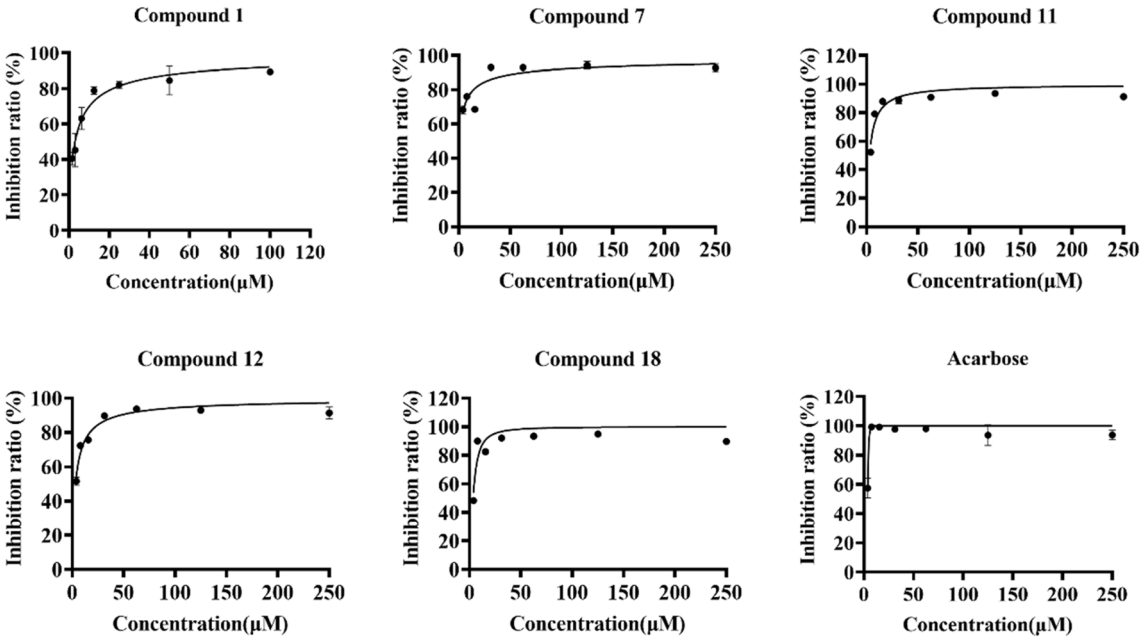

Fig. 4 Inhibitory activities of compounds **1**, **7**, **11**, **12**, **18**, and acarbose. Each point means the average ± standard deviation of triplicate measurements.

Table 4 IC_{50} for all isolated compounds and acarbose

Compounds	IC_{50} ± SD (μM)	Compounds	IC_{50} ± SD (μM)	Compounds	IC_{50} ± SD (μM)
1	3.03 ± 0.15	**9**	6.10 ± 0.04	**17**	21.38 ± 1.35
2	16.65 ± 1.01	**10**	9.48 ± 0.55	**18**	3.55 ± 0.45
3	>100	**11**	2.85 ± 0.15	**19**	>100
4	>100	**12**	3.16 ± 0.21	**20**	>100
5	>100	**13**	15.55 ± 0.53	**21**	>100
6	5.32 ± 0.08	**14**	4.84 ± 0.22	Acarbose	3.70 ± 0.20
7	1.13 ± 0.26	**15**	8.21 ± 0.34		
8	42.7 ± 9.00	**16**	4.24 ± 0.35		

 © 2025 The Author(s). Published by the Royal Society of Chemistry

Open Access Article. Published on 02 December 2025. Downloaded on 1/15/2026 7:05:29 AM.
This article is licensed under a Creative Commons Attribution-NonCommercial 3.0 Unported Licence.

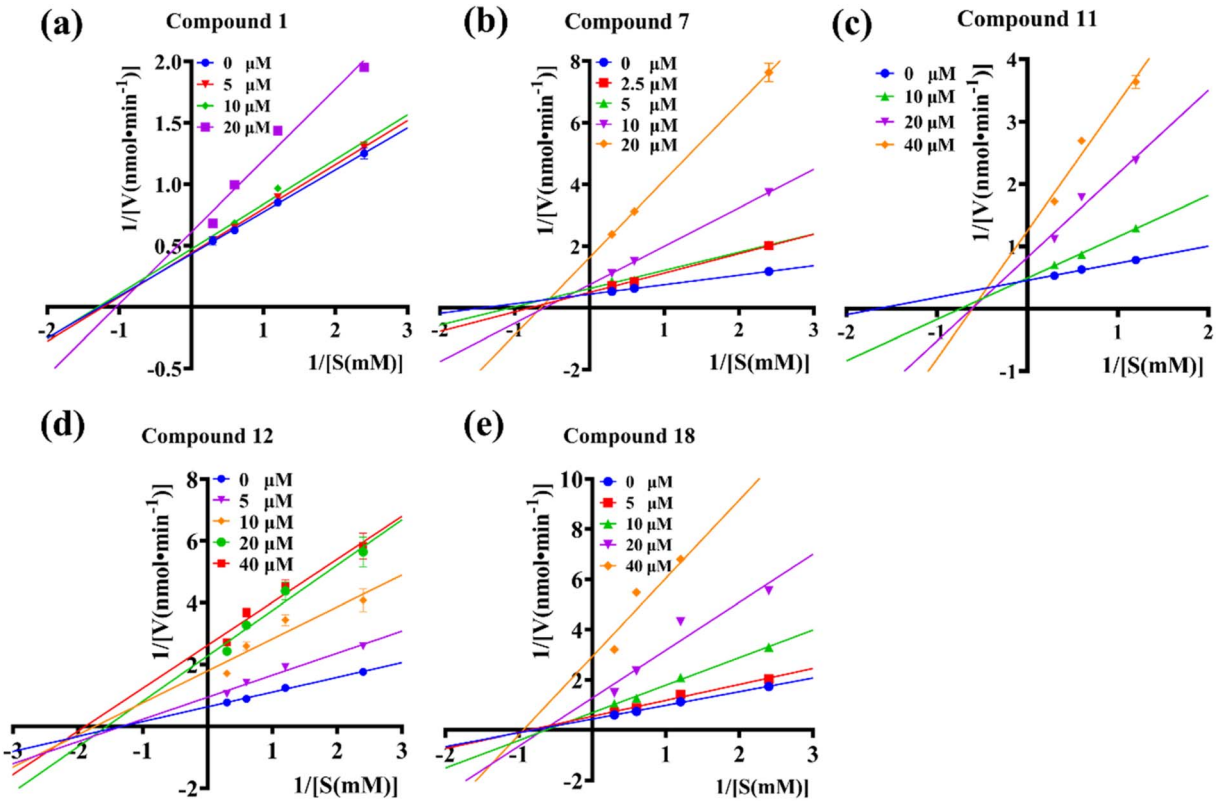

Fig. 5 Lineweaver–Burk plots (a–e) of compounds 1, 7, 11, 12, and 18 for the α-glucosidase respectively.

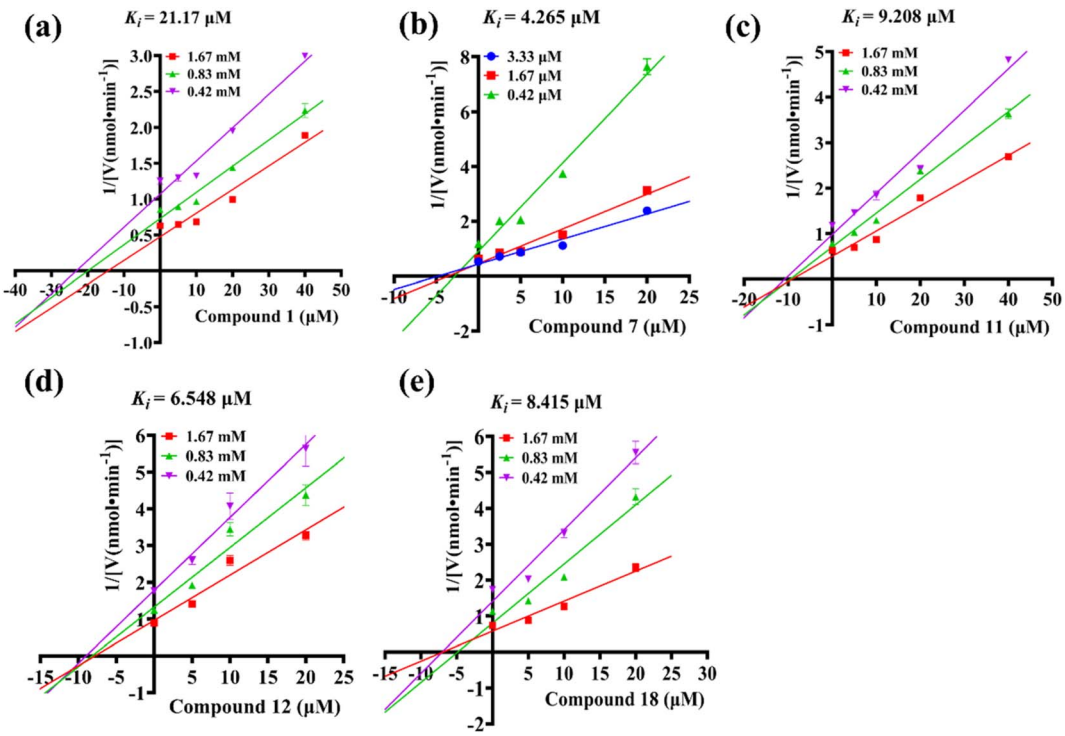

Fig. 6 Dixon plots [a–e] of compounds 1, 7, 11, 12, and 18 for the α-glucosidase respectively.

Open Access Article. Published on 02 December 2025. Downloaded on 1/15/2026 7:05:29 AM.
This article is licensed under a Creative Commons Attribution-NonCommercial 3.0 Unported Licence.

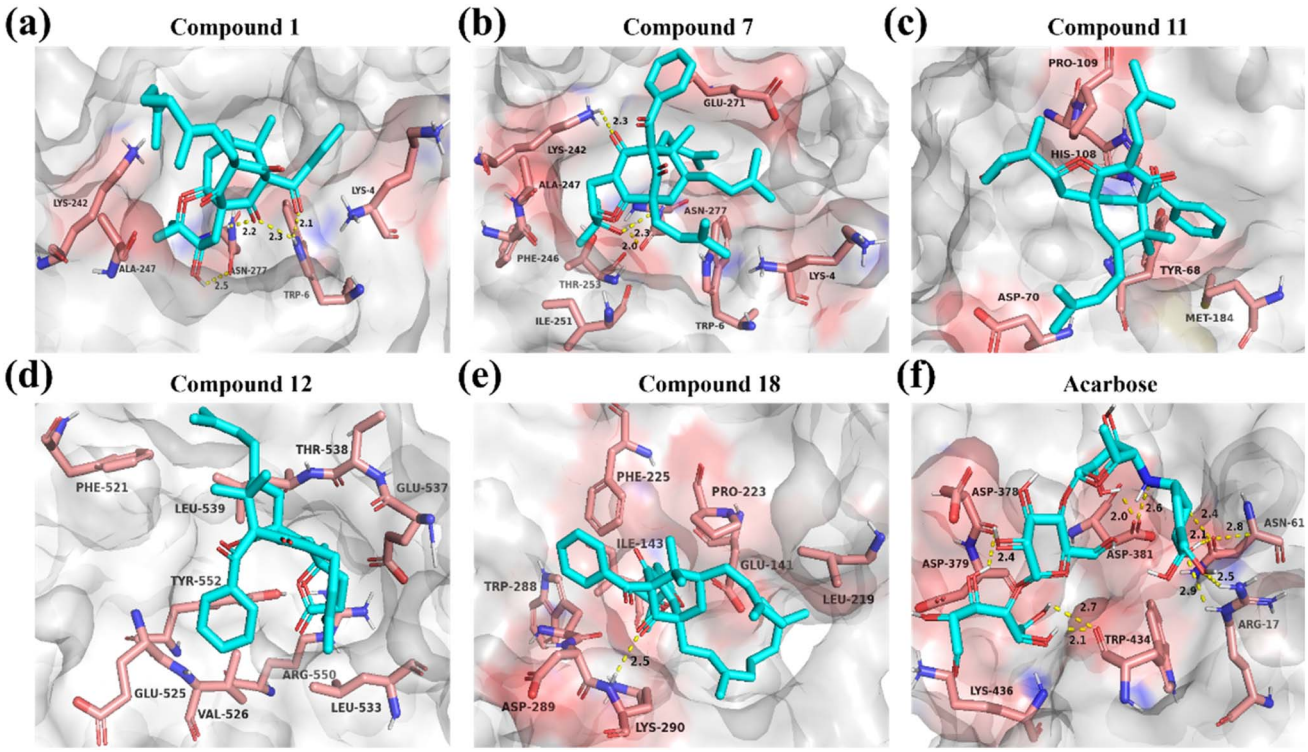

Fig. 7 Molecular binding mode of compounds **1** (a), **7** (b), **11** (c), **12** (8), **18** (e), and acarbose (f) with α-glucosidase.

Pro223, Phe225, Trp288, and Asp289. Additionally, the five compounds (**1**, **7**, **11**, **12**, and **18**) with better inhibitory effects than the positive control (acarbose) had lower binding energies to α-glucosidase (−7.3, −7.3, −8.2, −7.5, −7.1 kcal mol^{-1}, respectively) than that of acarbose (−5.8 kcal mol^{-1}).

3. Conclusion

In this study, **21** compounds including seven undescribed compounds were obtained from the fruit of *Hypericum addingtonii* N. Robson. The activity studies showed that compounds **1**, **7**, **11**, **12**, and **18** had stronger α-glucosidase inhibitory activity than acarbose. The structure–activity relationship analysis indicated that most of the meroterpenoid derivatives isolated from the fruit of *Hypericum addingtonii* N. Robson effectively inhibited α-glucosidase, except for compounds **3–5**. This suggests that meroterpenoid derivatives have an advantage over anthrone derivatives for inhibiting α-glucosidase. Moreover, by comparing the structure and activity of compounds **3–5** to compounds **6** and **7**, the pyran ring was found to be important for activity. Our present study showed that the fruit of *Hypericum addingtonii* N. Robson contains high levels of meroterpenoid derivatives, which have anti-diabetic properties and can be consumed to promote health in T2DM.

4. Experimental

4.1 General procedures

High-resolution mass spectrometry (HR-MS) or tandem mass spectrometry (MS/MS analyses) were conducted using high-pressure liquid chromatography coupled with quadrupole time-of-flight mass spectrometry (HPLC-Q-TOF-MS) with a dual Agilent jet stream electrospray ionization source (6540, Agilent, USA). An infrared (IR) spectrometer and ultraviolet (UV)-2600 spectrometer (Affinity-1, Shimadzu, Japan) were used to obtain the IR and UV spectra. All optical rotations were measured using a polarimeter (Paar MCP 500, France, Anton) at 25 °C. All nuclear magnetic resonance (NMR) data were obtained using an NMR spectrometer (400 MHz, Bruker BioSpin Group, Switzerland). All of the chemical shifts were recorded with respect to the deuterated solvent shift ($CDCl_3$: δ_H 7.26 for the proton resonance and δ_C 77.0 for the carbon; $(CD)_3CO$: δ_H 2.05 for the proton resonance and δ_C 29.8 and 206.3 for the carbon). A C_{18} column (Cosmosil, 5 μm, 20 × 250 mm) was used for semi-preparative HPLC. Octadecylsilyl (ODS, 50 μm, YMC), silica gel, Sephadex LH-20 (Pharmacia, Kalamazoo, MI, USA), and MCI gel (CHP20P, Japan) were used for column chromatography.

4.2 Plant materials

The fruit of *Hypericum addingtonii* N. Robson was obtained from Yunnan Province, China. After being identified by Prof. Aijia Ji (Guangzhou University of Chinese Medicine), an identical sample (No. 2019091001) was preserved at Guangzhou University of Traditional Chinese Medicine, Guangzhou, China.

4.3 Extraction and isolation

The air-dried fruit of *Hypericum addingtonii* N. Robson (10 kg) was powdered and extracted three times using ethanol (EtOH,

 © 2025 The Author(s). Published by the Royal Society of Chemistry

Open Access Article. Published on 02 December 2025. Downloaded on 1/15/2026 7:05:29 AM. This article is licensed under a Creative Commons Attribution-NonCommercial 3.0 Unported Licence.

70%) at 90 °C to produce 3.6 kg of residue. The residue was dissolved in a mixture of ethyl acetate (EtOAc) and water and then the two layers were separated. The EtOAc residue (300 g) was separated into seven fractions (Fr. 1–7) using silica gel column chromatography with a PE–EtOAc (1 : 0 to 0 : 1, v/v) solvent system.

Fr. 4 was separated into Fr. 4A to 4F using an MCI gel column. Compounds **3** (10.3 mg) and **4** (19.3 mg) were isolated from Fr. 4C using a Sephadex column (methanol, MeOH) and HPLC preparation. Fr. 4E was separated into Fr. 4E-1 to 4E-4 using a Sephadex column. Compound **5** (24.8 mg) was afforded from Fr. 4E-2 using semi-preparative HPLC.

Fr. 5 was separated into Fr. 5A to 5I using an MCI column. Then, Fr. 5D was separated into Fr. 5D-1 to Fr. 5D-7 using an ODS column eluted with MeOH. Compound **19** (12.4 mg) was isolated from Fr. 5D-5 using HPLC preparation. Compounds **2** (112.0 mg), **10** (40.7 mg), **13** (33.9 mg), **14** (24.8 mg), **15** (5.5 mg), **16** (121.8 mg), **20** (8.1 mg), and **21** (10.2 mg) were obtained from Fr. 5D-6 using semi-preparative HPLC. Compounds **8** (10.8 mg), **9** (23.5 mg), and **17** (42.2 mg) were obtained from Fr. 5E using a Sephadex column and HPLC preparation. Compounds **1** (10.8 mg), **6** (54.5 mg), **7** (10.6 mg), and **18** (118.2 mg) were obtained from Fr. 5F using a Sephadex column and HPLC preparation.

Fr. 6 was separated into Fr. 6A to 6J using the MCI column. Compounds **11** (11.4 mg) and **12** (13.3 mg) were obtained from Fr. 6H using a Sephadex LH-20 column and HPLC preparation.

4.3.1 Hypertonii A (1). Yellow oil; $[\alpha]_D^{25}$ +42.3 (c 0.1, CH_3CN); IR (KBr) ν_{max} cm^{-1} 2966, 2925, 1733, 1684, 1447, 1393, 1373, 1247, 1222, 1185,1134, 686 cm^{-1}; UV (CH_3CN): λ_{max} nm (log ε) 194 (1.8), 247 (0.6), 281 (0.2); ECD (CH_3CN) λ_{max} nm ($\Delta\varepsilon$) 220 (+6.7), 230 (+2.08), 251 (+6.43), 305 (−0.81), 332 (−2.90). HRESIMS *m/z* 561.3210 $[M + H]^+$ (calcd for $C_{35}H_{45}O_6^+$: 561.3211); NMR data see Tables 1 and 2.

4.3.2 Hypertonii B (2). Colorless oil; $[\alpha]_D^{25}$ +30.6 (c 0.1, CH_3CN); IR (KBr) ν_{max} cm^{-1} 2967, 2928, 2869, 1705, 1663, 1653, 1596, 1457, 1381, 1267, 1126, 1072, 1024, 694; UV (CH_3CN): λ_{max} nm (log ε) 192 (8.2), 248 (0.85), 281 (0.34); ECD (CH_3CN) λ_{max} nm ($\Delta\varepsilon$) 210 (+25.9), 248 (+2.64), 274 (−0.65), 297 (+1.77), 355 (+0.79). HRESIMS *m/z* 561.3938 $[M + H]^+$ (calcd for $C_{37}H_{54}O_4^+$, 561.3938); NMR data see Tables 1 and 2.

4.3.3 Hypertonii C (3). Yellow oil; $[\alpha]_D^{25}$ +25.4 (c 0.1, CH_3CN); IR (KBr) ν_{max} 2960, 2930, 2870, 1687, 1636, 1438, 1458, 1386, 1363, 1233, 1069, 995 cm^{-1}, UV (CH_3CN): λ_{max} (log ε) 198 (3.5), 250 (1.4), 272 (1.2) nm; ECD (CH_3CN) λ_{max} nm ($\Delta\varepsilon$) 205 (+4.29), 220 (−6.84), 246 (+3.85), 266 (−3.29), 323 (+0.62). $[M + H]^+$ *m/z* 655.3857 (calcd for $C_{38}H_{55}O_9^+$, 655.3841); NMR data see Tables 1 and 2.

4.3.4 Hypertonii D (4). Yellow oil; $[\alpha]_D^{25}$ +18.6 (c 0.1, CH_3CN); IR (KBr) ν_{max} 2977, 2928, 1735, 1698, 1596, 1447, 1373, 1248, 1223, 1149, 1127, 1035, 688 cm^{-1}, UV (CH_3CN): λ_{max} (log ε) 198 (3.5), 250 (1.4), 272 (1.2) nm; ECD (CH_3CN) λ_{max} nm ($\Delta\varepsilon$) 204 (+5.49), 219 (−5.99), 247 (+5.33), 267 (−2.73), 333 (+0.97). $[M + H]^+$ *m/z* 655.3856 (calcd for $C_{38}H_{54}O_9$, 655.3841); NMR data see Tables 1 and 2.

4.3.5 Hyperxanthone G (19). Yellow oil; $[\alpha]_D^{25}$ −43.6 (c 0.1, CH_3CN); IR (KBr) ν_{max} 2926, 2362, 1718, 1710, 1684, 1609, 1559, 1457, 1148 cm^{-1}; UV (CH_3CN): λ_{max} (log ε) 240 (1.74), 277 (3.3), 330 (1.7) nm; ECD (CH_3CN) λ_{max} nm ($\Delta\varepsilon$) 204 (−0.54), 218 (+2.50), 251 (−0.13), 272 (+1.39), 286 (+0.39), 299 (−0.20), 315 (+0.05). $[M - H]^-$ *m/z* 301.0716 (calcd for $C_{16}H_{13}O_6^-$, 301.0718); NMR data see Table 3.

4.3.6 Hyperxanthone H (20). Yellow oil; $[\alpha]_D^{25}$ −43.6 (c 0.1, CH_3CN); IR (KBr) ν_{max} 2926, 2362, 1718, 1710, 1684, 1609, 1559, 1457, 1148 cm^{-1}; UV (CH_3CN): λ_{max} (log ε) 240 (1.74), 277 (3.3), 330 (1.7) nm; $[M + H]^+$ *m/z* 311.0904 (calcd for $C_{18}H_{17}O_5$, 311.0914); NMR data see Table 3.

4.3.7 Hyperxanthone I (21). Yellow oil; $[\alpha]_D^{25}$ −24.5 (c 0.1, CH_3CN); IR (KBr) ν_{max} 3420, 2923, 2362, 2344, 1718, 1700, 1647, 1603, 1465, 1382, 1269, 1161, 1090, 830 cm^{-1}; UV (CH_3CN): λ_{max} (log ε) 179 (6.8), 222 (4.7), 243 (4.2), 263 (7.6), 323 (3.3) nm; $[M + H]^+$ *m/z* 327.1225 (calcd for $C_{19}H_{19}O_5$, 327.1229); ^1H and ^{13}C NMR data see Table 3.

4.4 Electronic circular dichroism (ECD) calculations

Prior to the calculations, the conformations for compounds **1–4** and **19** were searched using Spartan 14 software with a Merck molecular force field.[26] The primary conformers were identified based on the Boltzmann distribution rate and then optimized and simulated based on time-dependent density-functional theory (TD-DFT) method using Gaussian 09 software.[27] After the calculations, SpecDis 1.6 software was used to extract the heat and ECD spectra of all conformers and sum the spectra.[28] Gauge-including atomic orbital (GIAO) NMR calculations were performed under the mPW1PW91 functional and 6-31 + G (d, p) level using a polarizable continuum model for solvation in chloroform. The computational details of all conformers are provided in the appendix.

4.5 $[Mo_2(OAc)_4]$-induced circular dichroism

Weigh an appropriate amount of the compound to be tested and dissolve it in anhydrous dimethyl sulfoxide (DMSO) to prepare a solution with a concentration of approximately 0.8 mol L^{-1}. Measure its CD spectrum using anhydrous DMSO as the blank. Dissolve the sample solution in pre-weighed $Mo_2(OAc)_4$, with the molar ratio of sample to $Mo_2(OAc)_4$ being approximately 1 : 1.2. Subtracting the CD spectrum of the complex from that of the sample eliminates any signal from the sample itself. Observe signs of Cotton effects in the difference spectrum within a range of 300–310 nm and determine the absolute conformation of adjacent diols.

4.6 Assessment of biological activity

4.6.1 α-Glucosidase inhibitory activity. The α-glucosidase inhibitory activities of all isolated compounds were evaluated by measuring the hydrolysis rate of α-glucosidase to its substrate (*p*-nitrophenyl-α-D-glucopyranoside, *p*-NPG). Briefly, all compounds were dissolved in 50% dimethysulfoxide and then diluted to a series of concentrations. The α-glucosidase enzyme was suspended in potassium phosphate buffer (pH = 6.8, 0.06 U mL^{-1}), and the substrate (*p*-NPG) was dissolved in double distilled water (5 mM). To prepare the test group, the test samples (3 μL) were combined with *p*-NPG (100 μL) and then 150 μL of enzyme solution (0.06 U mL^{-1}) was added. The control

Open Access Article. Published on 02 December 2025. Downloaded on 1/15/2026 7:05:29 AM.
This article is licensed under a Creative Commons Attribution-NonCommercial 3.0 Unported Licence.

group was prepared without the test sample and the blank control was prepared without the test sample and enzyme solution. All the reaction mixtures were added to 300 μL of potassium phosphate buffer and reacted at 37 °C for 20 min. The reaction was terminated by increasing the temperature to 95 °C for 5 min. After centrifugation, 70 μL of supernatant and 130 μL of sodium carbonate solution (0.1 M, pH 11.0) were added to a 96-well plate, and the absorbance values were measured using a microplate reader at 405 nm. The inhibitory rate (IR) was calculated as IR (%) $= 1 - [(A_t - A_b)/(A_c - A_b)] \times 100\%$, where A_c, A_b and A_t are the absorbance values of the control, blank, and test groups, respectively. Each sample was performed in triplicate. Acarbose was used as the positive control.

4.7 Kinetic analysis for inhibition type

The kinetic constants (K_m and V_{max}) and inhibition mechanism of compounds **1**, **7**, **11**, **12**, and **18** were analyzed using kinetic analysis. First, the IR was tested using different substrate concentrations (3.33–0.21 mM of *p*-NPG) and compound concentrations for the Dixon plots (single reciprocal plots) and Lineweaver–Burk plots. The test concentrations used were from 0 to 40 μM for **1**, **11**, **12**, and **18**, and from 0 to 20 μM for **7**. GraphPad Prism 5.0 software (GraphPad Software, Inc., La Jolla, CA, USA) was used for analyzsis.

4.8 Molecular docking

The molecular docking was displayed on Autodock software (1.5.6). The crystal structure of α-glucosidase (Protein Data Bank (PDB) ID: 5zcb) was downloaded from the PDB database. The 3D structures of all compounds were constructed with energy minimization using ChemDraw3D software.

Conflicts of interest

The authors declare that they have no known competing financial interests or personal relationships that could have influenced the work reported in this study.

Data availability

Supplementary information (SI): key ROSEY correlations of **1–4**. Experimental and calculated ECD spectra of **19**. Regression analysis of experimental and calculated ^{13}C NMR data of **3** and **4**. α-Glucosidase inhibitory effect. ECD calculation details of **1–4**. 1D and 2D NMR, HRESIMS, IR, and UV of **1**−**4** and **19–21**. See DOI: https://doi.org/10.1039/d5ra05247e.

Acknowledgements

This work was financially supported by the Scientific research project of Guangdong Provincial Bureau of TCM (20231117), and Science and Technology Projects in Guangzhou (No. 202201011559), Guangdong Provincial Key Laboratory of Research on Emergency in TCM (2023B1212060062).

References

1 A.-Z. Wang, H. Han, Q.-Q. Fang and C.-H. Tan, *Phytochemistry*, 2023, **205**, 113482.
2 Y.-P. Liu, Y.-J. Li, Y.-Y. Zhao, J.-M. Guo, Y.-Y. Liu, X.-P. Wang, Z.-Y. Shen, L. Qiang and Y.-H. Fu, *Bioorg. Chem.*, 2021, **110**, 104775.
3 C. Liang, L. Kjaerulff, P. R. Hansen, K. T. Kongstad and D. Staerk, *J. Nat. Prod.*, 2021, **84**, 2454–2467.
4 T. Sriyatep, I. Siridechakorn, W. Maneerat, A. Pansanit, T. Ritthiwigrom, R. J. Andersen and S. Laphookhieo, *J. Nat. Prod.*, 2015, **78**, 265–271.
5 O. O. Johnson, M. Zhao, J. Gunn, B. D. Santarsiero, Z. Q. Yin, G. A. Ayoola, H. A. B. Coker and C. T. Che, *J. Nat. Prod.*, 2016, **79**, 224–229.
6 A. Raksat, P. Phukhatmuen, J. Yang, W. Maneerat, R. Charoensup, R. J. Andersen, Y. A. Wang, S. G. Pyne and S. Laphookhieo, *J. Nat. Prod.*, 2020, **83**, 164–168.
7 Y.-X. Zhang, Z. Ao, Y.-W. He, J.-Y. Lu, X.-L. Chen, L.-Y. Kong and J.-G. Luo, *Fitoterapia*, 2021, **155**, 105063.
8 S. Chatterjee, K. Khunti and M. J. Davies, *Lancet*, 2017, **389**, 2239–2251.
9 J. Harreiter and M. Roden, *Wien. Klin. Wochenschr.*, 2019, **131**, 6–15.
10 B. Zhang, Z. Deng, D. D. Ramdath, Y. Tang, P. X. Chen, R. Liu, Q. Liu and R. Tsao, *Food Chem.*, 2015, **172**, 862–872.
11 X. Peng, G. Zhang, Y. Liao and D. Gong, *Food Chem.*, 2016, **190**, 207–215.
12 Z.-B. Zhou, Z.-R. Li, X.-B. Wang, J.-G. Luo and L.-Y. Kong, *J. Nat. Prod.*, 2016, **79**, 1231–1240.
13 X.-Q. Chen, Y. Li, X. Cheng, K. Wang, J. He, Z.-H. Pan, M.-M. Li, L.-Y. Peng, G. Xu and Q.-S. Zhao, *Chem. Biodivers.*, 2010, **7**, 196–204.
14 N. Kondo, T. Kuroda and D. Kobayashi, *Int. J. Mol. Sci.*, 2021, **22**, 10922.
15 M. L. Castro, A. M. do Nascimento, M. Ikegaki, C. M. Costa-Neto, S. M. Alencar and P. L. Rosalen, *Bioorg. Med. Chem.*, 2009, **17**, 5332–5335.
16 C. J. Chua-Aguilera, B. Möller and N. Yawalkar, *Clin. Rev. Allergy Immunol.*, 2017, **53**, 371–393.
17 H. Zhu, C. Chen, Q. Tong, X. Chen, J. Yang, J. Liu, B. Sun, J. Wang, G. Yao, Z. Luo, Y. Xue and Y. Zhang, *Sci. Rep.*, 2015, **5**, 14772.
18 J. S. Smolen, D. Aletaha and I. B. McInnes, *Lancet*, 2016, **388**, 2023–2038.
19 Z. Zhou, Y. Zhang, K. Pan, J. Luo and L. Kong, *Fitoterapia*, 2014, **95**, 1–7.
20 P. Phukhatmuen, A. Raksat, S. Laphookhieo, R. Charoensup, T. Duangyod and W. Maneerat, *Heliyon*, 2020, **6**, e03625.
21 M. Górecki, E. Jabłońska, A. Kruszewska, A. Suszczyńska, Z. Urbańczyk-Lipkowska, M. Gerards, J. W. Morzycki, W. J. Szczepek and J. Frelek, *J. Org. Chem.*, 2007, **72**, 2906–2916.
22 Z. B. Zhou, Z. R. Li, X. B. Wang, J. G. Luo and L. Y. Kong, *J. Nat. Prod.*, 2016, **79**, 1231–1240.

 © 2025 The Author(s). Published by the Royal Society of Chemistry

Open Access Article. Published on 02 December 2025. Downloaded on 1/15/2026 7:05:29 AM.
This article is licensed under a Creative Commons Attribution-NonCommercial 3.0 Unported Licence.

23 T.-T. Liu, X.-J. Liao, S.-H. Xu and B.-X. Zhao, *Nat. Prod. Res.*, 2021, **35**, 3780–3786.
24 N. Tanaka, Y. Takaishi, Y. Shikishima, Y. Nakanishi, K. Bastow, K.-H. Lee, G. Honda, M. Ito, Y. Takeda, O. K. Kodzhimatov and O. Ashurmetov, *J. Nat. Prod.*, 2004, **67**, 1870–1875.
25 M. T. Ha, T. H. Lee, C. S. Kim, R. Prajapati, J. A. Kim, J. S. Choi and B. S. Min, *Phytochemistry*, 2022, **197**, 113100.
26 *Spartan'14*, Wavefunction, Inc., Irvine, CA, 2013.
27 *Gaussian 09W*, Gaussian, Inc., Wallingford, CT, 2010.
28 T. Bruhn, A. Schaumlöffel, Y. Hemberger and G. Bringmann, *SpecDis, Version 1.63*, University of Würzburg, Würzburg, Germany, 2015.